Thomas, B.G., "Continuous Casting: Complex Models," *The Encyclopedia of Materials: Science and Technology*, K.H. J. Buschow, R. Cahn, M. Flemings, B. Ilschner, E. J. Kramer, S. Mahajan, eds., (J. Dantzig, subject ed.) Elsevier Science Ltd., Oxford, UK, Vol. 2, 2001, pp. 1599-1609, and at http://www.elsevier.com/mrwclus/15/show/Main.htt

Continuous Casting: Complex Models

Continuous casting is used to solidify most of the 750 million tons of steel, 20 million tons of aluminum, and many tons of other alloys produced in the world every year. Most previous advances have been based on empirical knowledge gained from experimentation with the process. As computer power increases, mathematical models are becoming increasingly powerful tools to gain additional quantitative insight.

Model applications include basic machine design calculations, identifying and quantifying the mechanisms of various types of defects, troubleshooting the origin of particular defects, and optimizing the various process conditions to increase productivity or minimize defects. This article discusses recent examples of these models with emphasis on the different phenomena that have been modeled in steel continuous casting, comparison with experiments, and practical implications of the findings.

1. Basic Phenomena and Modeling

Like most commercial processes, continuous casting involves a staggering complexity of interacting phenomena at the mechanistic level. Some of the important phenomena include:

- fully-turbulent, transient fluid motion in a complex geometry (inlet nozzle and strand liquid pool), affected by argon gas bubbles, thermal and solutal buoyancies
- thermodynamic reactions within and between the powder and steel phases
- flow and heat transport within the liquid and solid flux layers, which float on the top surface of the steel
- dynamic motion of the free liquid surfaces and interfaces, including the effects of surface tension, oscillation and gravity-induced waves, and flow in several phases
- transport of superheat through the turbulent molten steel
- transport of solute (including intermixing during a grade change)

- transport of complex-geometry inclusions through the liquid, including the effects of buoyancy, turbulent interactions, and possible entrapment of the inclusions on nozzle walls, gas bubbles, solidifying steel walls, and the top surface
- thermal, fluid, and mechanical interactions in the meniscus region between the solidifying meniscus, solid slag rim, infiltrating molten flux, liquid steel, powder layers, and inclusion particles.
- heat transport through the solidifying steel shell, the interface between shell and mold, (which contains powder layers and growing air gaps) and the copper mold.
- mass transport of powder down the gap between shell and mold
- distortion and wear of the mold walls and support rolls
- nucleation of solid crystals, both in the melt and against mold walls
- solidification of the steel shell, including the growth of grains and microstructures, phase transformations, precipitate formation, and microsegregation
- shrinkage of the solidifying steel shell, due to thermal contraction, phase transformations, and internal stresses
- stress generation within the solidifying steel shell, due to external forces, (mold friction, bulging between the support rolls, withdrawal, gravity) thermal strains, creep, and plasticity (which varies with temperature, grade, and cooling rate)
- crack formation, due to internal stresses and composition-dependent ductility problems
- coupled segregation, on both microscopic and macroscopic scales

Because of this complexity, no model can include all of the phenomena at once. An essential aspect of successful model development is the selection of the key phenomena of interest to a particular modeling objective and the making of reasonable assumptions. These crucial phenomena should be treated mechanistically, in order to accurately reproduce them. Mechanistic models are based on satisfying the laws of conservation of heat, mass, force and momentum in an appropriate domain with appropriate boundary conditions. Each phenomenon considered is represented by term(s) in these governing equations. Other phenomena can be ignored or incorporated using empirical constants, obtained through experimentation and model calibration. The equations are discretized using finite difference or finite element methods and are solved numerically with computers, which are becoming increasingly fast and affordable.

2. Solidification and Heat Transfer

In the continuous casting process, illustrated in Figure 1, molten metal is delivered from the bottom of a transfer vessel (the tundish) into a mold cavity. Here, the water-cooled walls of the mold extract heat to solidify a shell that contains the liquid pool. The shell is withdrawn from the bottom of mold at a "casting speed" that matches the inflow of metal, so that the process ideally operates at steady state. Below the mold, water sprays extract heat from the surface, and the strand core eventually becomes fully solid when it reaches the "metallurgical length".

Heat flow / solidification models are used for basic design and troubleshooting of this process. These models solve the transient heat conduction equation

$$\rho(\partial H / \partial t + \mathbf{v} \bullet \nabla H) = \nabla \bullet \left(k_{eff} \nabla T\right) + Q \qquad [1]$$

The temperature, T, depends on the temperature-dependent material properties of effective thermal conductivity, k_{eff}, and density, ρ, the velocity field, **v**, various heat sources, Q, and the boundary conditions. Latent heat evolution and heat capacity are incorporated into the constitutive equation that must also be supplied to relate temperature, T, with enthalpy, H.

Axial heat conduction can be ignored in models of steel continuous casting because it is small relative to axial advection, as indicated by the small Peclet number (casting-speed multiplied by shell thickness divided by thermal diffusivity). Thus, Lagrangian models of a horizontal slice through the strand have been employed with great success for steel. Aluminum continuous casting has a short metallurgical length, owing to its high thermal conductivity and slow casting speed, so this assumption cannot be made. See Dantzig_Modeling_and_Scaling_article for details on how decisions like these are made.

Heat transfer in the mold region is controlled mainly by heat conduction across the interface between the surface of the solidifying shell and the mold. The greatest difficulty in accurate heat flow modeling is determination of the heat transfer across this gap, q_{gap}, which varies with time and position depending on the thickness, d_{gap}, and the properties of the gas or lubricating flux layers that fill it, such as k_{gap}.

$$q_{gap} = \left(h_{rad} + \frac{k_{gap}}{d_{gap}} \right) \left(T_{0shell} - T_{0mold} \right) \qquad [2]$$

Where metal shrinkage is not matched by taper of the mold walls, an air gap can form, especially in the corners. This greatly reduces the heat flow. Advanced models simulate the mold, interface,

and shell, and use shrinkage models to predict the size of this gap, d_{gap}. In steel slab casting operations with mold flux, such models feature a detailed treatment of the interface, including heat, mass, and momentum balances on the flux in the gap and the effect of shell surface imperfections (oscillation marks) on heat flow and flux consumption (Thomas, Ho et al., 1998). The coupled effect of flow in the molten metal on delivering superheat to the inside of the shell and thereby retarding solidification is also modeled. Mold heat flow models can be used to identify deviations from normal operation and thus predict quality problems such as impending breakouts or surface depressions in time to take corrective action.

Heat flow models which extend below the mold are needed for basic machine design to ensure that the last support roll and torch cutter are positioned beyond the metallurgical length for the highest casting speed. Below the mold, surface temperature of the strand is maintained by air mist and water spray cooling, while the interior solidifies. Online open-loop dynamic cooling models can be employed to control the spray flow rates in order to ensure uniform surface cooling even during transients, such as the temporary drop in casting speed during a nozzle change. A heat flow model can also be used to troubleshoot defects. For example, the location of a misaligned support roll that may be generating internal hot-tear cracks can be identified by matching the position of the start of the crack beneath the strand surface with the location of solidification front down the caster calculated with a calibrated model.

3. Fluid Flow in the Mold

Flow in the mold is of great interest because it influences many important phenomena, which have far-reaching consequences on strand quality. These effects include the dissipation of superheat (and temperature at the meniscus), the flow and entrainment of the top surface powder layers, top-surface contour and level fluctuations, and the entrapment of subsurface inclusions and gas bubbles. Design compromises are needed to simultaneously satisfy the contradictory requirements for avoiding each of these defect mechanisms.

Some of the important phenomena which govern the continuous casting of steel and determine the quality of the product are illustrated in Figure 2. Steel flows into the mold through ports in the submerged entry nozzle, which is usually bifurcated. Nozzle geometry greatly affects the flow in the mold and is easy to change, so is an important subject of mathematical modeling.

The jet leaving the nozzle flows across the mold and impinges against the shell solidifying at the narrow face. The flow pattern depends on the casting conditions. It also can fluctuate with time,

leading to intermittent defects, so transient behavior is important. Figure 3 shows an instantaneous image of the flow pattern in the mold cavity calculated with a direct numerical solution of the Navier-Stokes equations,

$$\rho \mathbf{v} \bullet \nabla \mathbf{v} = -\nabla p + \nabla \bullet \left(\mu \nabla \mathbf{v} + \nabla \mathbf{v}^T \right) + \mathbf{S} \qquad [3]$$

The calculations are compared with particle image velocimetry measurements of the flow in a water model, shown on the right side of Figure. These calculations reveal structures in the flow pattern that are important to transient events such as the intermittent capture of inclusion particles.

Although transient calculations can provide detailed insights, the computational cost can be greatly reduced using a turbulence model such as K-ε to approximate the steady time-averaged flow pattern. This model increases the effective viscosity so allows a much coarser mesh. However, it generally requires the solution of two additional conservation equations for the transport of turbulent kinetic energy and its dissipation, which are sometimes inaccurate.

The flow pattern changes radically with increasing argon injection rate (Thomas, Huang et al., 1994) or with the application of electromagnetic forces (Ishii, Sazhin et al., 1996), which can either brake or stir the liquid. These phenomena add significant complexity to the equations that must be solved for the flow model.

4. Superheat Dissipation

An important task of the flow pattern is to deliver molten steel to the meniscus region that has enough superheat during the critical first stages of solidification. Superheat is the sensible heat of the liquid metal above the liquidus temperature.

The dissipation of superheat is modeled by solving Eq. 1 using the velocities found from the flow model (Eq. 3). The effective thermal conductivity of the liquid is proportional to the effective viscosity, which depends on the turbulence parameters. The solidification front, which forms the boundary to the liquid domain, can be treated in different ways. Some researchers model flow and solidification as a coupled problem on a fixed grid. Although very flexible, this approach is subject to convergence difficulties and requires a fine grid to resolve the thin porous mushy zone.

An alternative approach for columnar solidification of a thin shell, such as found in the continuous casting of steel, is to treat the boundary as a rough wall fixed at the liquidus temperature using

"wall laws" (Huang, Thomas et al., 1992). Figure 4 compares calculations using this approach with measured temperatures in the liquid pool. Incorporating the effects of argon on the flow pattern was very important in achieving the reasonable agreement observed. This figure shows that the temperature drops almost to the liquidus by mold exit, indicating that most of the superheat is dissipated in the mold. Most of this heat is delivered to the narrow face where the jet impinges, which is important to shell solidification.

The coldest regions are found at the meniscus at the top corners near the narrow face and near the SEN. This is a concern because it could lead to freezing of the meniscus, and encourage solidification of a thick slag rim. This could lead to quality problems such as deep oscillation marks, cracks and other surface defects. In the extreme, the steel surface can solidify a solid bridge between the SEN and the shell against the mold wall, which often causes a breakout. To avoid these problems, flow must reach the surface quickly. These calculations should be used, for example, in designing nozzle port geometries that do not direct the flow too deep.

5. Top Surface Powder / Flux Layer Behavior

The flow of steel in the upper mold may influence the top surface powder layers, which are very important to steel quality. Mold powder is added periodically to the top surface of the steel. It sinters and melts to form a protective liquid flux layer, which helps to trap impurities and inclusions. This liquid is drawn into the gap between the shell and mold, where it acts as a lubricant and helps to make heat transfer more uniform. These phenomena are difficult to measure or to accurately simulate with a physical model, so are worthy of mathematical modeling.

Figure 5 shows results from a 3-D finite-element model of heat transfer and fluid flow in the powder and flux layers. The bottom of the model domain is the steel / flux interface. Its shape is imposed based on measurements in an operating caster. Alternatively, this interface shape can be calculated by solving additional equations to satisfy the force balance at the interface, which involves the pressure in the two phases, shear forces from the moving fluids, and surface tension, and gravity (Panaras, Theodorakakos et al., 1998). For the conditions in this figure, the momentum of the flow up the narrow face has raised the level of the interface there. The shear stress along the interface is determined through coupled calculations with the 3-D steady flow model. The model features different temperature-dependent flux properties for the interior, where the flux viscosity during sintering before melting, compared with the region near the narrow face mold walls, where the flux resolidifies to form a solid rim.

When molten steel flows rapidly along the steel / flux interface, it induces motion in the flux layer. If the interface velocity becomes too high, then the liquid flux can be sheared away from the interface, become entrained in the steel jet, and be sent deep into the liquid pool to become trapped in the solidifying shell as a harmful inclusion. If the interface velocity increases further, then the interface standing wave becomes unstable, and huge level fluctuations contribute to further problems.

The thickness of the beneficial liquid flux layer is also very important. As shown in the model calculations in Figure 5, the liquid flux layer may become dangerously thin near the narrow face if the steel flow tends to drag the liquid towards the center. This shortage of flux feeding into the gap can lead to air gaps, reduced, non-uniform heat flow, thinning of the shell, and longitudinal surface cracks. Quantifying these phenomena requires modeling of both the steel flow and flux layers.

6. Motion and Entrapment of Inclusions and Gas Bubbles

The jets of molten steel exiting the nozzle may carry argon bubbles and inclusions such as alumina into the mold cavity. These particles may create defects if they become entrapped in the solidifying shell. Particle trajectories can be calculated using the Lagrangian particle tracking method, which solves a transport equation for each particle as it travels through a previously-calculated velocity field. The force balance on each particle includes buoyancy and drag force relative to the steel. The effects of turbulent motion can be modeled crudely from a K-ε flow field by adding a random velocity fluctuation at each step, whose magnitude varies with the local turbulent kinetic energy level. To obtain significant statistics, the trajectories of several hundred individual particles should be calculated, using different starting points. The bubbles collect inclusions, and inclusion clusters collide, so their size and shape distributions evolve with time, which affects their drag and flotation velocities and importance. Models are being developed to include these effects (Thomas, Dennisov et al., 1997).

Figure 6 shows the trajectories of several particles moving through a steady flow field, calculated using the K-ε model. Most of the argon bubbles circulate in the upper mold area and float out to the top surface. A few might be trapped at the meniscus if there is a solidification hook, and lead to surface defects. A few small bubbles manage to penetrate into the lower recirculation zone, where they move similarly to large inclusion clusters. Particles in this lower region tend to move slowly in large spirals, while they float towards the inner radius of the slab. When they eventually touch the solidifying shell in this deep region, entrapment is more likely on the inside radius.

Trapped argon bubbles elongate during rolling and in low-strength steel, may expand during subsequent annealing processes to create costly surface blisters and “pencil pipe" defects. Transient models are likely to yield further insights into the complex and important phenomena of inclusion entrapment.

7. Composition Variation During Grade Changes

Large composition differences can arise through the thickness and along the length of the final product due to intermixing after a change in steel grade during continuous casting. Steel producers need to optimize casting conditions and grade sequences to minimize the amount of steel downgraded or scrapped due to this intermixing. In addition, the unintentional sale of intermixed product must be avoided. To do this requires knowledge of the location and extent of the intermixed region and how it is affected by grade specifications and casting conditions.

Models to predict intermixing must first simulate composition change exiting the tundish as a function of time. For small tundish operations, mixing in the liquid core of the strand must also be calculated. These calculations can be done using simple lumped mixing-box models and / or by solving the mass diffusion equation in the flowing liquid:

$$\partial C/\partial t + \mathbf{v} \bullet \nabla \mathbf{C} = \nabla \bullet \left(D_{eff} \nabla \mathbf{C} \right) \qquad [4]$$

In this equation, the composition, C, ranges between the old grade concentration of 0 and the new grade concentration of 1. This dimensionless concept is useful because alloying elements intermix essentially equally, owing to the much greater importance of turbulent convection over laminar diffusion. In order to predict the final composition distribution within the final product, a further model must account for the cessation of intermixing after the shell has solidified.

Intermix models have been developed for both slab and bloom casting (Huang and Thomas, 1996; Thomas, 1997) and are in use at several companies. Such models can be enhanced to serve as on-line tools by outputting for each grade change, the critical distances which define the length of intermixed steel product which falls outside the given composition specifications for the old and new grades. In addition, they can be applied off-line to perform parametric studies to evaluate the relative effects on the amount of intermixed steel for different intermixing operations and for different operating conditions using a standard ladle-exchange operation. Finally, they can be used to optimize scheduling and casting operation to minimize cost.

8. Thermal Mechanical Behavior of the Mold

Thermal distortion of the mold during operation is important to residual stress, residual distortion, fatigue cracks, and mold life. By affecting the internal geometry of the mold cavity, it is also important to the size of the gap that controls heat transfer to the solidifying shell. To study thermal distortion of the mold, 3-D elastic-plastic-creep finite element models have been developed for slabs (Thomas, Li et al., 1998) and thin slabs (O'Conner and Dantzig, 1994) using ABAQUS. In order to match the measured distortion, models should incorporate all of the important geometric features of the mold, which often includes the four copper plates with their water slots, reinforced steel water box assemblies, and tightened bolts. Its four-piece construction makes a slab mold behave very differently from a single-piece bloom or billet mold, which have also been studied using thermal stress models (Samarasekera, Anderson et al., 1982). This type of stress model application will become more important in the future to optimize the design of the new molds being developed for continuous thin-slab and strip casting. In twin-roll strip casting, for example, thermal distortion of the rolls during operation is on the same order as the section thickness of the steel product.

9. Thermal Mechanical Behavior of the Shell

The solidifying shell is prone to a variety of distortion and crack problems, owing to its creep at elevated temperature, combined with metallurgical embrittlement and thermal stress. To investigate these problems, models have been developed to simulate coupled thermal and mechanical behavior of a solidifying steel shell during continuous casting. The equations and solution procedures are documented elsewhere (Dantzig, 1989).

An example of the predicted temperature contours and distorted shape of a transverse region near the corner is compared in Figure 7 with measurements of a breakout shell from an operating steel caster. The model tracks the behavior of a two-dimensional slice through the strand as it moves downward at the casting speed through the mold and upper spray zones. It consists of separate finite-element models of heat flow and stress generation that are step-wise coupled through the size of the interfacial gap. The heat transfer model was calibrated using thermocouple measurements down the centerline of the wideface for typical conditions. Shrinkage predictions from the stress model are used to find the air gap thickness needed in Eq. 2 in order to extend the calculations around the mold perimeter. The model includes the effect of mold distortion on the air gaps, and

superheat delivery from the flowing jet of steel, calculated in separate models. The stress model includes ferrostatic pressure from the molten steel on the inside of the shell and calculates intermittent contact between the shell and the mold. It also features a temperature-dependent elastic modulus and an elastic-viscoplastic constitutive equation that includes the effects of temperature, composition, phase transformations and stress state on the local inelastic creep rate. Efficient numerical algorithms are needed to integrate the equations.

As expected, good agreement is obtained in the region of good contact along the wideface, where calibration was done. Near the corner along the narrow face, steel shrinkage is seen to exceed the mold taper, which was insufficient. Thus, an air gap is predicted. This air gap lowers heat extraction from the shell in the off-corner region of the narrow face. When combined with high superheat delivery from the bifurcated nozzle directed at this location, shell growth is greatly reduced locally. Just below the mold, this thin region along the off-corner narrow-face shell caused the breakout.

Near the center of the narrow face, creep of the shell under ferrostatic pressure from the liquid is seen to maintain contact with the mold, so much less thinning is observed. This illustrates the tremendous effect that superheat has on slowing shell growth, if there is a problem which lowers heat flow.

Figure 8 presents sample distributions of temperature and stress through the thickness of the shell, calculated with this model. To achieve reasonable accuracy, a very fine mesh and small time steps are needed. The temperature profile is almost linear through the shell. The stress profile shows that the shell surface is in compression. This is because, in the absence of friction with the mold, the surface layer solidifies and cools stress free. As each inner layer solidifies, it cools and tries to shrink, while the surface temperature remains relatively constant. The slab is constrained to remain planar, so complementary subsurface tension and surface compression stresses are produced. To maintain force equilibrium, note that the average stress through the shell thickness is zero. It is significant that the maximum tensile stress is found near the solidification front. This generic subsurface tensile stress is responsible for hot tear cracks, when accompanied by metallurgical embrittlement.

This model has been applied to predict ideal mold taper, to prevent breakouts such as the one discussed here (Lawson, Sander et al., 1994) and to understand the cause of other problems such as surface depressions (Thomas, Moitra et al., 1996) and longitudinal cracks in slabs. Crack formation is particularly difficult to model directly. Very small strains can start hot tear cracks at

the grain boundaries if liquid metal is unable to feed through the secondary dendrite arms to accommodate the shrinkage. Strain localization may occur on both the small scale (when residual elements segregate to the grain boundaries) and on a larger scale (within surface depressions or hot spots). Later sources of tensile stress (including constraint due to sticking, unsteady cooling below the mold, bulging, and withdrawal) worsen strain concentration and promote crack growth. Microstructure, grain size and segregation are not generally included in a stress model, so modeling these phenomena is difficult. Thus, careful experiments are needed to determine the fracture criteria empirically. A typical experiment applies stress during solidification, which is difficult to control. Thus, detailed modeling of the experiment itself is becoming necessary, in order to extract new fundamental material properties.

Much further work is needed to understand and quantify these phenomena and to apply the results to optimize the continuous casting process. In striving towards these goals, the importance of combining modeling and experiments together cannot be overemphasized.

10. Future Frontiers

Mathematical models are growing in sophistication and thereby are becoming better able to quantify and understand the mechanisms of defect formation in processes such as continuous casting. Despite these advances, much more work is needed to quantify, incorporate, and simplify the key phenomena into better models before the use of mathematical models to design process improvements reaches its full potential and usefulness. In particular, more work is needed on transient phenomena and in better modeling of experiments to extract more fundamental material properties. It is crucial to emphasize that mathematical modeling tools must be used together with the other tools of the process engineer, which include laboratory and plant experimentation, physical models, and knowledge from previous experience.

Emerging continuous casting processes, such as thin slab and strip casting, present several special challenges, which offer opportunities for the application of mathematical models. With higher casting speeds and thinner mold cavities, these processes are more prone to fluid flow problems. Thinner product (with more surface) puts more demand on solving surface quality problems. The integration of casting and deformation processing together requires better understanding of the interaction between microstructure, properties, and processing. Conventional slab casting has had three decades of development and still is not perfected. For these new processes to thrive, the learning curve towards process optimization to produce quality steel needs to be shorter. As

computer hardware and software continue to improve, mathematical models will grow in importance as tools to meet this challenge.

See also: Samarasekera Continuous casting; McDavid Macroscopic modeling; Beckermann macrosegregation; Provatas Dendritic growth, etc.

Bibliography

Dantzig, J. A. (1989). "Thermal stress development in metal casting processes." Metallurgical Science and Technology **7**(3): 133-178.

Huang, X. and B. G. Thomas (1996). "Intermixing Model of Continuous Casting During a Grade Transition." Met. Trans. B **27B**(4): 617-632.

Huang, X., B. G. Thomas, et al. (1992). "Modeling Superheat Removal during Continuous Casting of Steel Slabs." Metall. Trans. B **23B**(6): 339-356.

Ishii, T., S. S. Sazhin, et al. (1996). "Numerical prediction of magnetohydrodynamic flow in continuous casting process." Ironmaking and Steelmaking **23**(3): 267-272.

Lawson, G. D., S. C. Sander, et al. (1994). Prevention of Shell Thinning Breakouts Associated with Widening Width Changes. Steelmaking Conference Proceedings. Warrendale, PA, Iron and Steel Society. : 329-336.

McDavid, R. and B. G. Thomas (1996). "Flow and Thermal Behavior of the Top-Surface Flux/ Powder Layers in Continuous Casting Molds." Metallurgical Transactions B **27B**(4): 672-685.

Moitra, A. and B. G. Thomas (1993). Application of a Thermo-Mechanical Finite Element Model of Steel Shell Behavior in the Continuous Slab Casting Mold. Steelmaking Proceedings. Dallas, TX, Iron and Steel Society. : 657-667.

O'Conner, T. and J. Dantzig (1994). "Modeling the Thin Slab Continuous Casting Mold." Metallurgical and Materials Transactions **25B**(4): 443-457.

Panaras, G. A., A. Theodorakakos, et al. (1998). "Numerical Investigation of the Free Surface in a continuous Steel Casting Mold Model." Metallurgical and Materials Transactions B **29B**(5): 1117-1126.

Samarasekera, I. V., D. L. Anderson, et al. (1982). "The Thermal Distortion of Continuous Casting Billet Molds." Met. Trans. B **13B**(March): 91-104.

Sivaramakrishnan, S., H. Bai, et al. (2000). Transient Flow Structures in Continuous Cast Steel. Steelmaking Conference Proceedings. Pittsburgh, PA, ISS, Warrendale, PA. .

Thomas, B. G. (1997). "Modeling Study of Intermixing in Tundish and Strand during a Continuous-Casting Grade Transition." ISS Transactions in Iron and Steelmaker **24**(12): 83-96.

Thomas, B. G. (2000). Continuous Casting of Steel, Chap. 15. Modeling and Simulation for Casting and Solidification: Theory and Applications. Marcel Dekker, New York. .

Thomas, B. G., A. Dennisov, et al. (1997). Behavior of Argon Bubbles during Continuous Casting of Steel. Steelmaking Conference Proceedings. Chicago, IL, ISS, Warrendale, PA. : 375-384.

Thomas, B. G., B. Ho, et al. (1998). Heat Flow Model of the Continuous Slab Casting Mold, Interface, and Shell. Alex McLean Symposium Proceedings, Toronto. Warrendale, PA, Iron and Steel Society. : 177-193.

Thomas, B. G., X. Huang, et al. (1994). "Simulation of Argon Gas Flow Effects in a Continuous Slab Caster." Metallurgical Transactions **25B**(4): 527-547.

Thomas, B. G., G. Li, et al. (1998). "Analysis of Thermal and Mechanical Behavior of Copper Molds during Continuous Casting of Steel Slabs." Iron and Steelmaker (ISS Transactions) **25**(10): 125-143.

Thomas, B. G., A. Moitra, et al. (1996). "Simulation of Longitudinal Off-Corner Depressions in Continuously-Cast Steel Slabs." ISS Transactions **23**(4): 57-70.

Thomas, B. G. and J. T. Parkman (1997). "Simulation of Thermal Mechanical Behavior during Initial Solidification." Thermec 97 Internat. Conf. on Thermomechanical Processing of Steel and Other Materials, Wollongong, Australia, TMS.

Brian G. Thomas
[Mechanical and Industrial Engineering, University of Illinois at Urbana-Champaign
1206 West Green Street, Urbana, IL 61801, U.S.A]

Figure Caption List

Fig. 1. Schematic of continuous casting processes

Fig. 2. Schematic of phenomena in the mold region of a steel slab caster

Fig. 3. Instantaneous flow pattern in a slab casting mold comparing LES simulation (left) and PIV measurement (right) (Sivaramakrishnan, Bai et al., 2000)

Fig. 4 Temperature distribution in mold showing superheat dissipation (Thomas, 2000)

Fig. 5. Comparison of measured and predicted melt-interface positions(McDavid and Thomas, 1996)

Fig. 6 Sample trajectories of five 208-micron solid alumina inclusion particles (Thomas, Dennisov et al., 1997)

Fig. 7 Comparison between predicted and measured shell thickness in a horizontal (x-y) section through the corner of a continuous-cast steel breakout shell (Moitra and Thomas, 1993)

Fig. 8 Typical Temperature and Stress distributions through shell thickness (Thomas and Parkman, 1997)

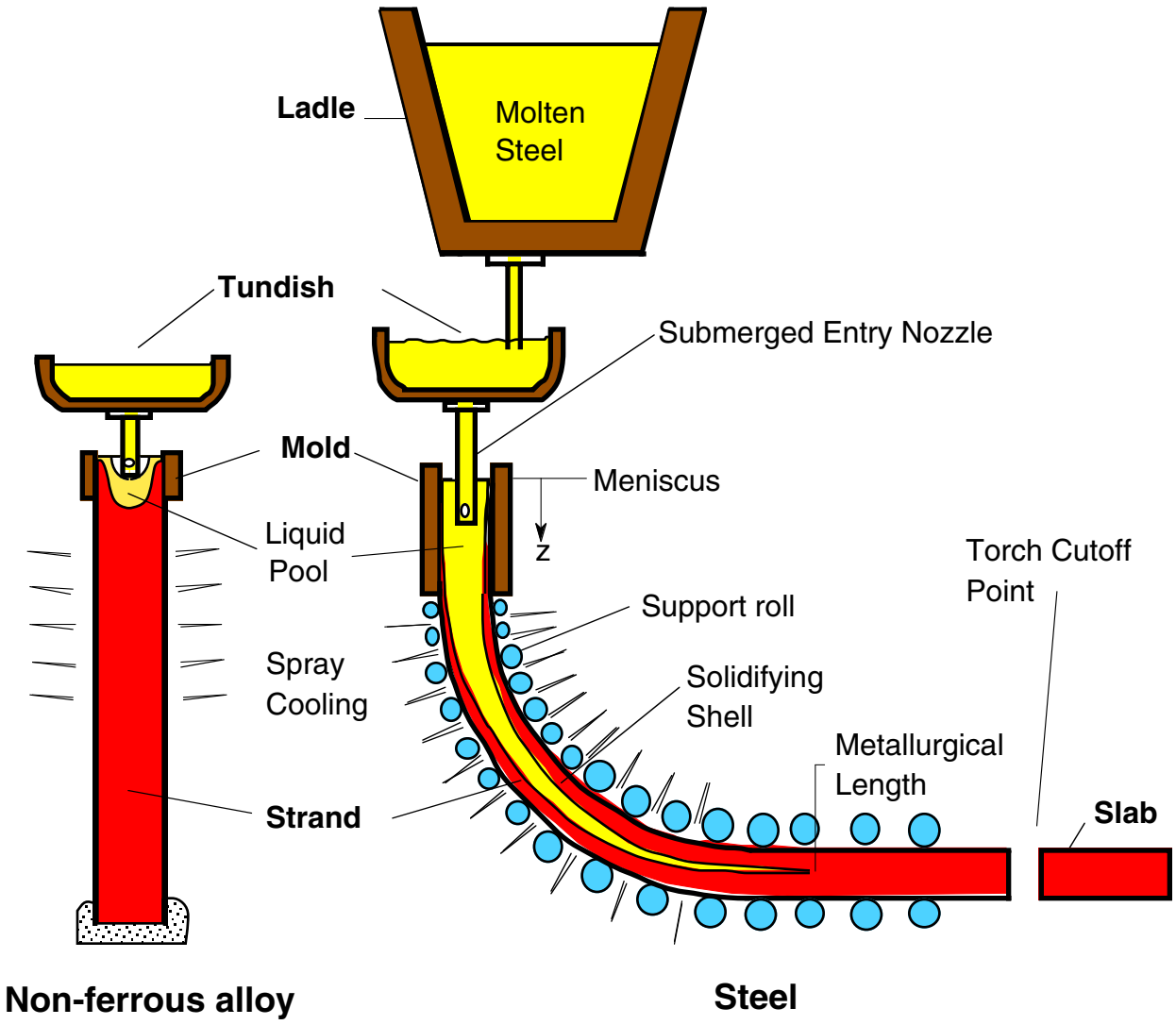

Figure 1. Schematic of continuous casting processes

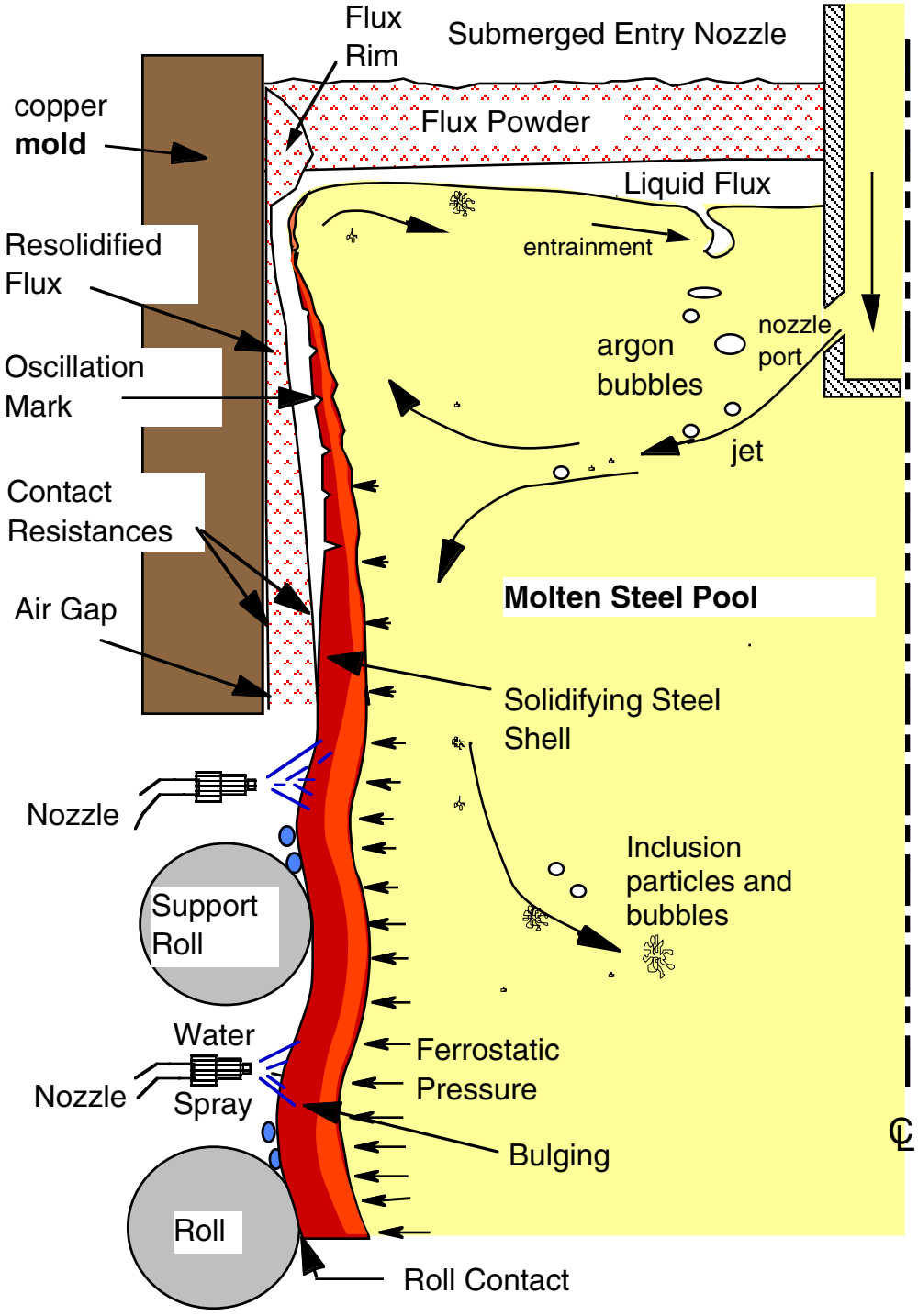

Figure 2. Schematic of phenomena in the mold region of a steel slab caster

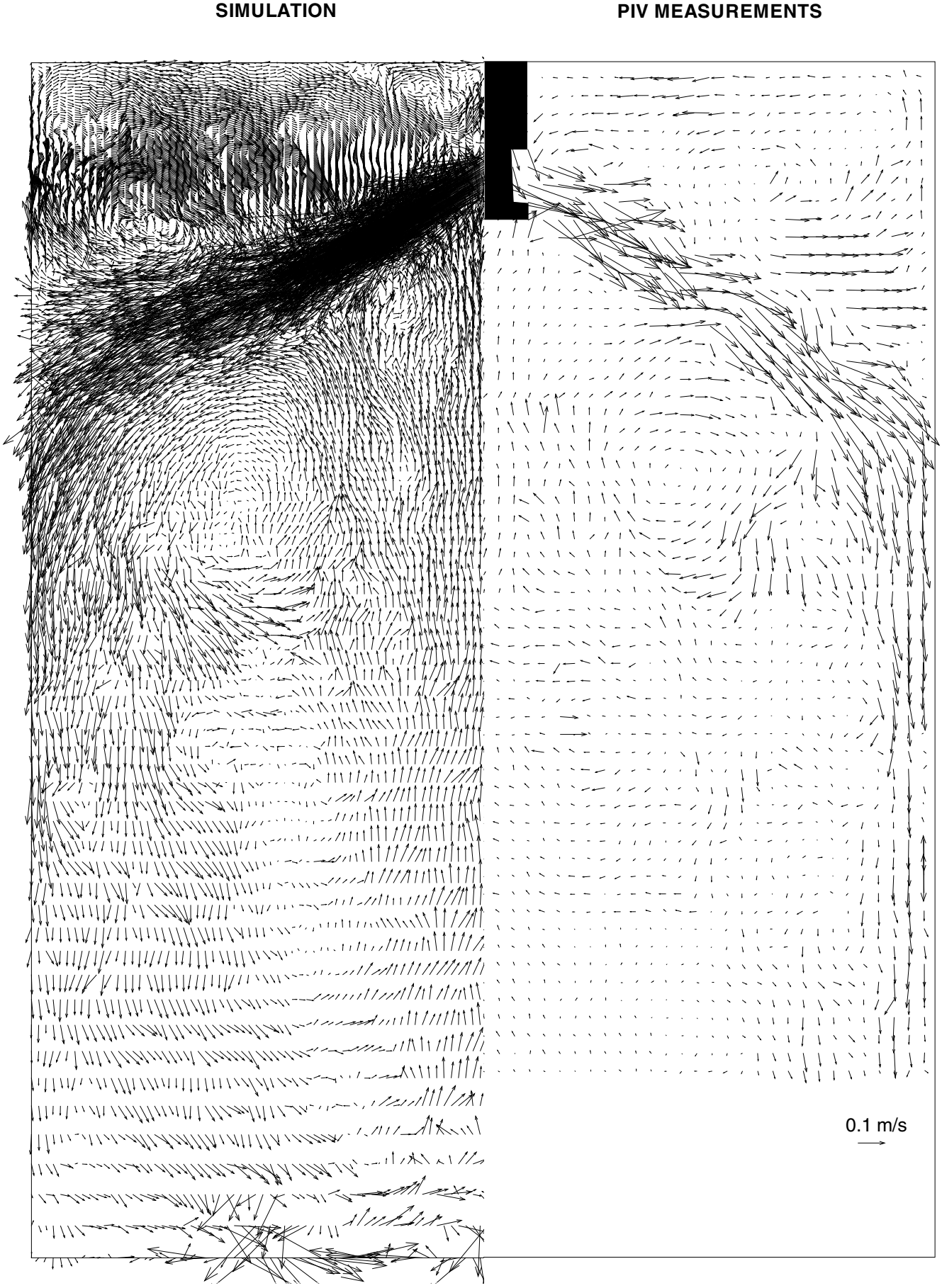

Figure 3 Instantaneous flow pattern in a slab casting mold comparing LES simulation (left) and PIV measurement (right) (Sivaramakrishnan, Bai et al., 2000)

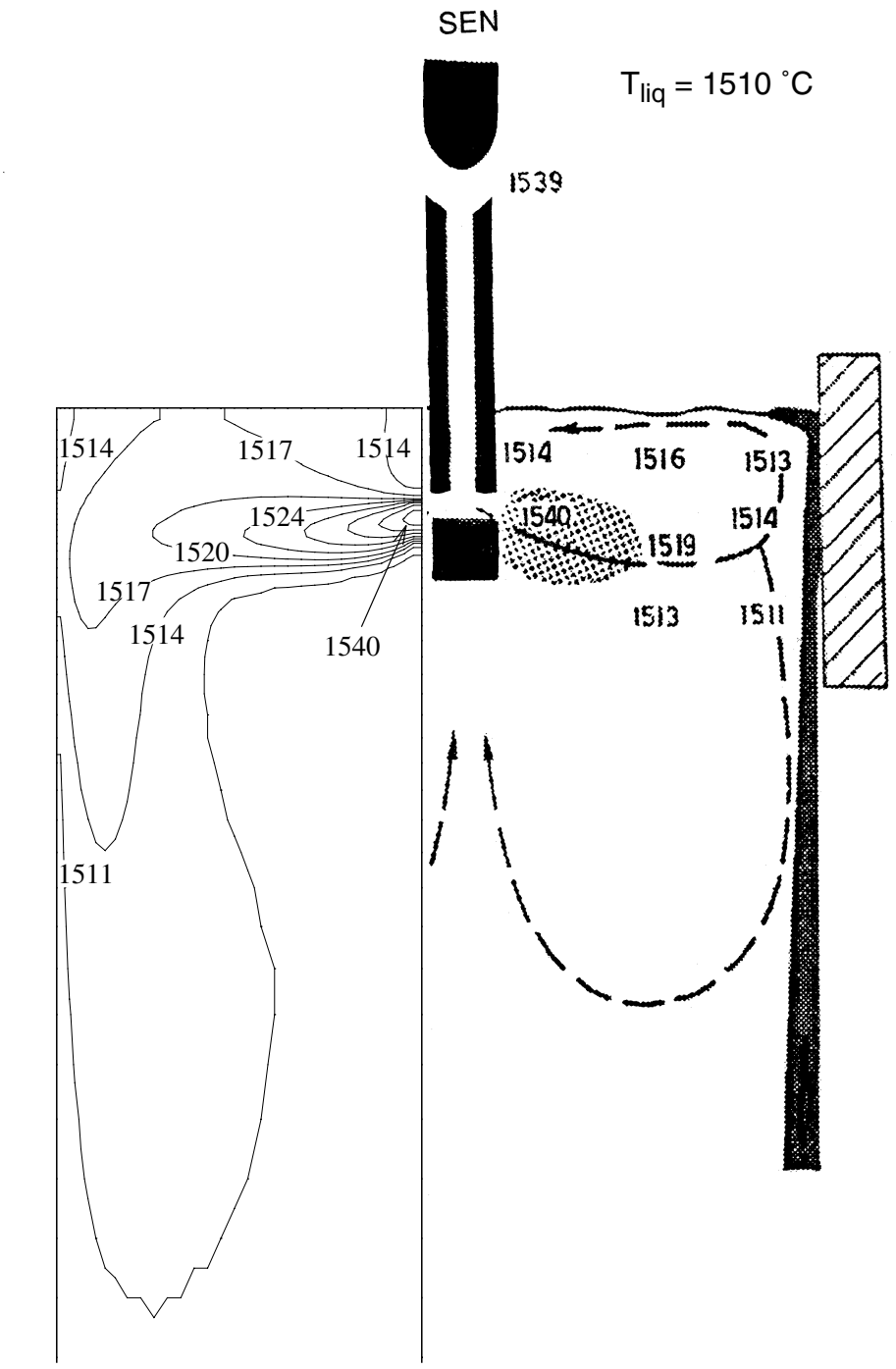

(a). Prediction (b). Experimental Measurement

Figure 4. Temperature distribution in mold showing superheat dissipation (Thomas, 2000)

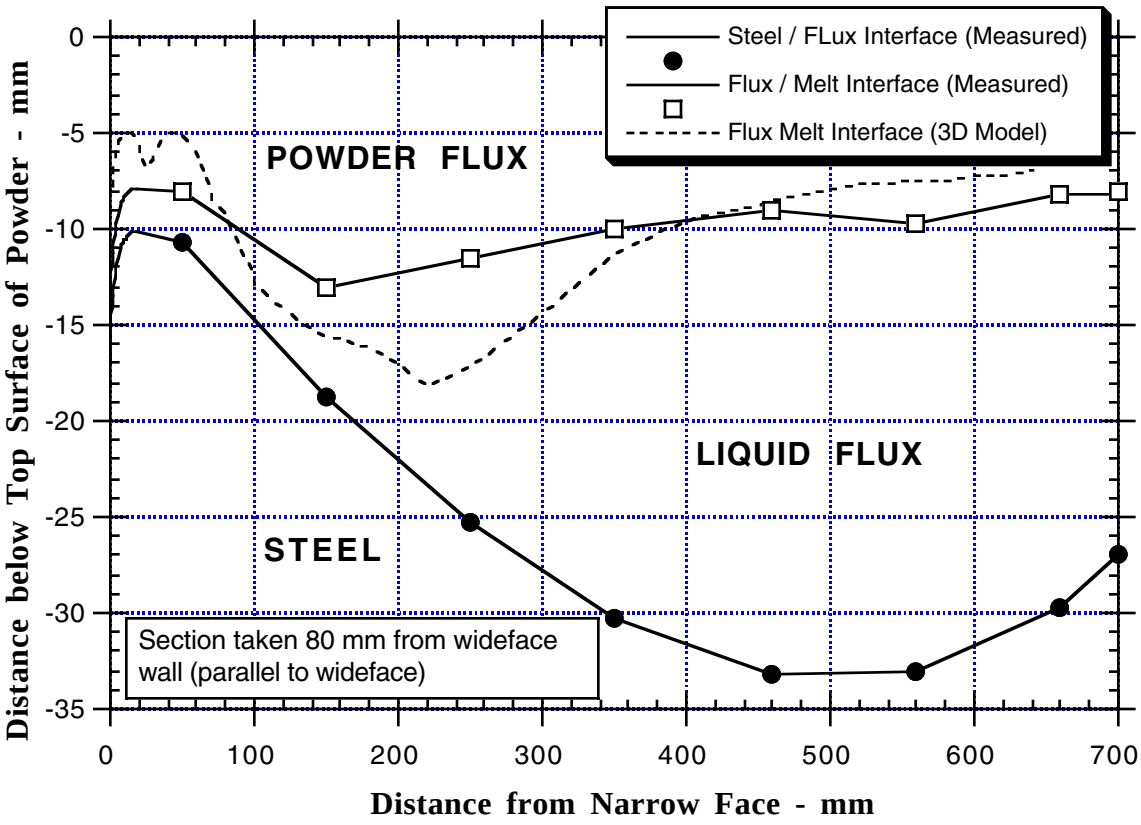

Figure 5. Comparison of measured and predicted melt-interface positions (McDavid and Thomas, 1996)

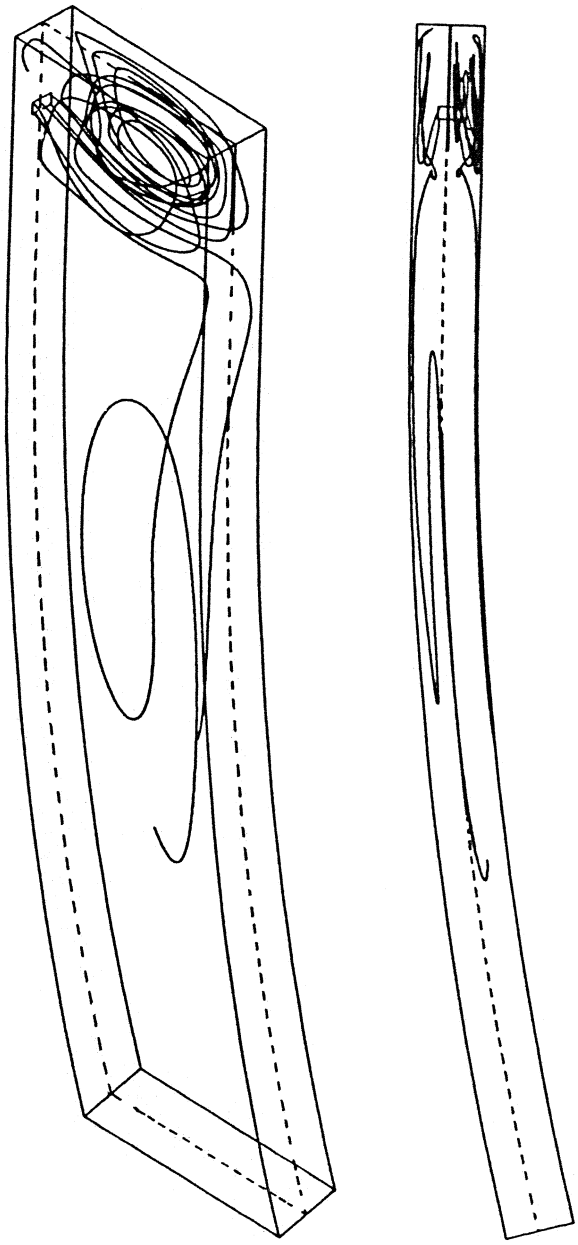

Figure 6. Sample trajectories of five 208-micron solid alumina inclusion particles (Thomas, Dennisov and Bai, 1997)

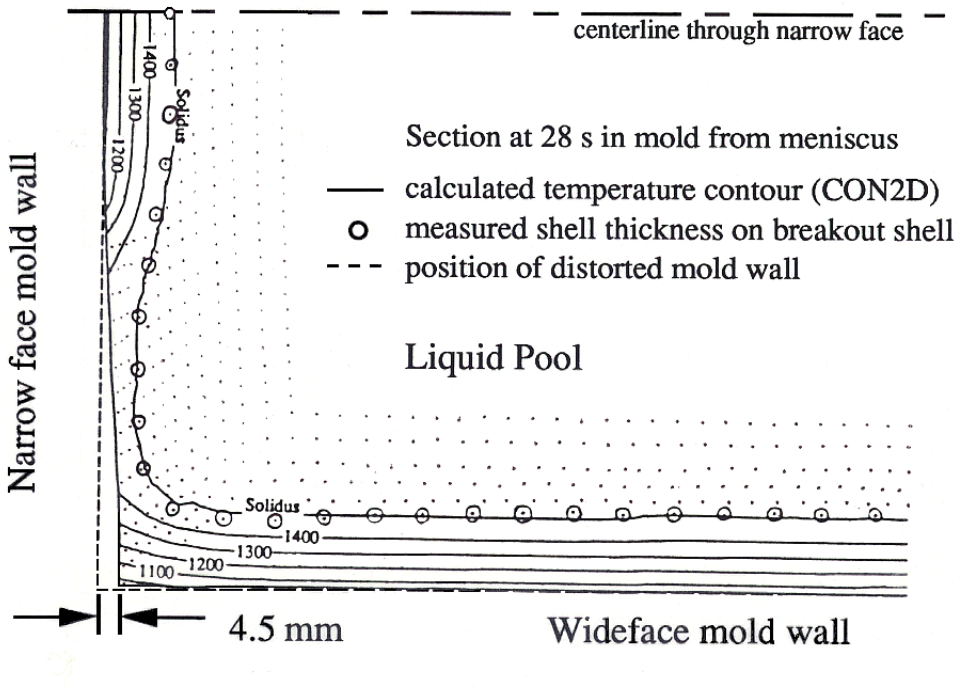

Figure 7. Comparison between predicted and measured shell thickness in a horizontal (x-y) section through the corner of a continuous-cast steel breakout shell (Moitra and Thomas, 1993)

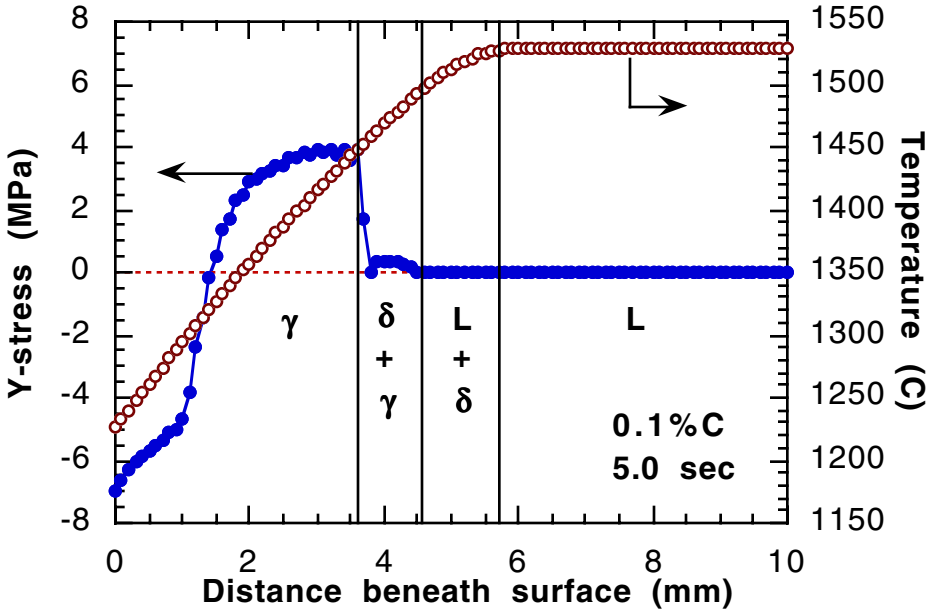

Figure 8. Typical Temperature and Stress distributions through shell thickness (Thomas and Parkman, 1997)